Water Resources Research

RESEARCH ARTICLE
10.1029/2019WR024757

Analytic Solutions for Tidal Propagation in Multilayer Coastal Aquifers

Mark Bakker[1]

[1]Water Resources Section, Faculty of Civil Engineering and Geosciences, Delft University of Technology, Delft, Netherlands

Key Points:
- Amplitude and phase shift of tidal signal can be computed analytically in multilayer coastal aquifers
- Aquifer system may extend below the sea and may include layers of low permeability
- Tidal signal propagates farther inland in deeper part of unconfined aquifers especially below thin clay lenses

Correspondence to:
M. Bakker,
mark.bakker@tudelft.nl

Citation:
Bakker, M. (2019). Analytic solutions for tidal propagation in multilayer coastal aquifers. *Water Resources Research*, *55*, 3452–3464. https://doi.org/10.1029/2019WR024757

Received 11 JAN 2019
Accepted 10 APR 2019
Accepted article online 15 APR 2019
Published online 29 APR 2019

Abstract A new analytic solution is presented for tidal propagation in multilayer coastal aquifers consisting of an arbitrary number of layers. The solution is derived using matrix calculus and may be applied to simulate tidal propagation in systems where aquifer layers are separated by leaky layers of low permeability or in stratified aquifers. The head, amplitude, and phase shift may be simulated for arbitrary tidal components. The transmissivity, storage coefficient, and loading efficiency may be different for every aquifer layer. Similarly, the resistance to vertical flow, storage coefficient, and loading efficiency may be different for every leaky layer. The aquifer system extends an infinite distance below the sea or may end abruptly at the shore line. In the former case, different aquifer and leaky layer properties may be specified below the sea and below the land. A homogeneous unconfined aquifer is simulated with 80 layers to demonstrate that the tidal signal propagates much farther inland in the deeper part than in the shallower part of an unconfined aquifer. This effect is enhanced significantly when layers of low permeability are present in the aquifer, even when these layers are fairly thin, such as clay lenses. The solution is implemented in Python and may be used, for example, to estimate aquifer parameters from head measurements in coastal aquifers.

1. Introduction

The principle of the tidal method is to use measurements of the tidal response in observation wells to estimate aquifer parameters (e.g., Carr & Van Der Kamp, 1969; Ferris, 1952). Measured heads are analyzed to determine the amplitude and phase shift of the major tidal components; corrections may be necessary to account for storage in observation wells (e.g., Hvorslev, 1951). Aquifer parameters, or combinations of aquifer parameters, are estimated by fitting an analytic solution for one specific tidal component. Many one-dimensional analytic solutions exist for single-layer coastal aquifers that end abruptly at the shore line; they are reviewed by Li and Jiao (2003). The focus of this paper is on aquifers that extend partially or completely below the sea.

Van der Kamp (1972) presented the first such solution; he considered a confined aquifer with an impermeable top that extends infinitely far below the sea. This solution was modified later for the case that the confining layer extends a finite distance below the sea with either a fixed head (Li & Chen, 1991) or a mixed boundary condition (Li et al., 2007) at the termination of the confining layer. Wang et al. (2012) presented a solution for a two-aquifer system separated by an impermeable layer where the top aquifer terminated at the shore line but the bottom aquifer extended a finite distance below the sea. A solution for the case of an aquifer covered by a leaky semiconfining layer without storage was presented by Chuang and Yeh (2007) for the case that the leaky layer extends infinitely far below the sea and by Li and Jiao (2001) for the case that the leaky layer extends a finite distance below the sea. The latter solution was modified by Chuang and Yeh (2008) by including a two-aquifer system in the land part of the system. Li et al. (2008) included storage in the leaky layer solution of Chuang and Yeh (2007). All solutions cited so far are for one-dimensional flow in coastal aquifers where the shore line is fixed and where the aquifer extends to infinity on the land side of the system. Many of these solutions are special cases of the multilayer solution presented here.

Several solutions or solution techniques have been developed for cases based on different approximations. Nielsen (1990) and Su et al. (2003) presented approximate analytic solutions for a sloping beach, where the shore line moves with the tide; Vandenbohede and Lebbe (2007) studied the effect of a sloping beach

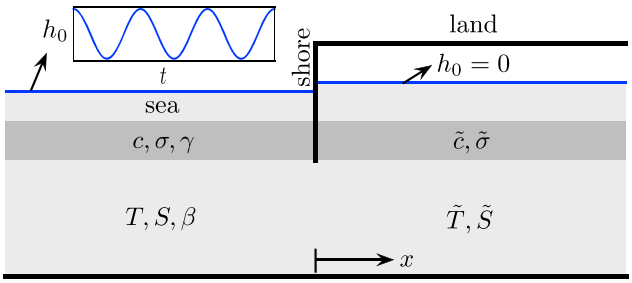

Figure 1. Cross section of a coastal aquifer extending below the sea.

with a numerical model. Maas and De Lange (1987) presented the solution for a tidal river with finite width, demonstrating the complex interaction of fluctuations caused by multiple boundaries. Rotzoll et al. (2008) and Sun et al. (2008) presented analytic solutions across long islands of finite width, again showing the effect of two boundaries. Teo et al. (2003) and Yeh et al. (2010) presented approximate analytic solutions for two-dimensional flow in a vertical cross section with a vertical beach on one side of the model and a water table condition at the top of the model. Bakker (2004) presented analytic element solutions for two-dimensional horizontal flow for coastlines of arbitrary shape, while Post (2011) created a MODFLOW package for periodic boundary conditions. Slooten et al. (2010) performed sensitivity analyses to determine where tidal fluctuations should be measured to obtain the most information. Besides the estimation of aquifer parameters, solutions for tidal fluctuations can be used to study, for example, the effect of tidal fluctuations on the spreading of solutes in coastal aquifers (e.g., Pool et al., 2014).

The objective of this paper is to present a new analytic solution for tidal fluctuations in a multilayer coastal aquifer consisting of an arbitrary number of layers. The aquifer system extends infinitely far below the sea; equations for aquifer systems that end abruptly at the shore are also provided but are not evaluated further. All layers can have different aquifer properties, which allows for the approximate modeling of phreatic conditions in the top layer of the aquifer system or the inclusion of thin clay lenses in sandy aquifers. First, the solution approach is introduced to derive the existing solution for a single aquifer, after which the solution approach is extended to an arbitrary number of layers. Examples are presented of the propagation of tidal effects in the deeper part of unconfined aquifers and of the effect of thin clay lenses on tidal propagation.

2. One-Dimensional Flow to a Shallow Sea With Tidal Fluctuations

Consider one-dimensional flow in an aquifer below and near a shallow sea with tidal fluctuations. The aquifer is covered by a leaky semiconfining layer. The resistance to vertical flow is neglected in the aquifer (Dupuit approximation), and flow in the leaky layer is approximated as vertical. The origin of the coordinate system is chosen at the shoreline (Figure 1). The aquifer below the sea extends to infinity along the negative x axis, and the aquifer below the land extends to infinity along the positive x axis. The transmissivity, storage coefficient, and loading efficiency of the aquifer below the sea are T, S, and β, respectively. The resistance to vertical flow, storage coefficient, and loading efficiency of the leaky layer below the sea are c, σ, and γ, respectively (Figure 1). Below the land, the transmissivity and storage coefficient of the aquifer are $\tilde{T}$ and $\tilde{S}$, respectively, and the resistance and storage coefficient of the leaky layer are $\tilde{c}$ and $\tilde{\sigma}$, respectively. The common approximation is adopted that horizontal deformations of the aquifer are neglected. Therefore, the loading efficiency is not defined for the aquifer below the land as the load there does not change. Unconfined flow in the aquifer below the land may be approximated by setting the storage coefficient equal to the specific yield, setting the resistance to $\tilde{c} = \infty$ so that no water leaks into the aquifer at the top, and by neglecting variations in the transmissivity (limitations of this approximation are discussed in, e.g., Sheets et al., 2015).

The head in the aquifer below the sea is governed by (e.g., Bakker, 2016; Van der Kamp, 1972)

$$T\frac{\partial^2 h}{\partial x^2} = S\frac{\partial h}{\partial t} + q_t - S\beta\frac{\mathrm{d}h_0}{\mathrm{d}t} \qquad x \le 0, \tag{1}$$

where β is the loading efficiency (also called tidal efficiency in studies of coastal aquifers), h is the head change caused by tidal fluctuations, and q_t is the vertical specific discharge at the top of the aquifer (positive when the water flows vertically upward). Flow in the aquifer below the land is obtained from (1) by setting the head h_0 above the aquifer equal to zero, which gives

$$\tilde{T}\frac{\partial^2 h}{\partial x^2} = \tilde{S}\frac{\partial h}{\partial t} + \tilde{q}_t \qquad x \ge 0. \tag{2}$$

Note that the case of nonzero but constant h_0 in the land portion of the aquifer can be solved by superposition.

Far from the shore, below the sea, the horizontal head gradient equals zero, while far from the shore below the land, the head equals zero.

$$\begin{aligned} \frac{\partial h}{\partial x} &= 0 \qquad x \to -\infty \\ h &= 0 \qquad x \to \infty. \end{aligned} \tag{3}$$

At the shore, the head and flow are continuous

$$\begin{aligned} h(0^-, t) &= h(0^+, t) \\ -T\frac{\partial h}{\partial x}(0^-, t) &= -\tilde{T}\frac{\partial h}{\partial x}(0^+, t), \end{aligned} \tag{4}$$

where 0^- and 0^+ indicate evaluation just to the left and right of $x = 0$, respectively.

A solution to the stated problem is sought in complex form. The water level in the sea $h_0(t)$ is therefore written in complex form as

$$h_0 = h_s e^{i\omega t}, \tag{5}$$

where h_s is the amplitude of the tide in the sea, i is the imaginary unit, and ω is defined as

$$\omega = 2\pi/\tau, \tag{6}$$

where τ is the period of the tide. The real part of (5) is equal to a sea level fluctuation

$$\Re h_0 = h_s \cos(\omega t), \tag{7}$$

while the imaginary part is equivalent to a sea level fluctuation

$$\Im h_0 = h_s \sin(\omega t). \tag{8}$$

In the remainder of this section, the head h is complex, where the real part is the response to a sea level that varies as a cosine function (7) and the imaginary part is the response to a sea level that varies as a sine function (8). A solution is sought in separable form

$$h = \phi e^{i\omega t}, \tag{9}$$

where $\phi = \phi(x)$ is a (complex) function of x only. The complex leakage q_t at the top of the aquifer below the sea may be written as a function of the head h_0 in the sea and the head h in the aquifer and the resistance and storage coefficient of the leaky layer as (see equation A15 in Appendix A):

$$q_t = gh - [f + (g - f)\gamma]h_0, \tag{10}$$

where f and g are given by equations A13 as

$$f = \frac{\sqrt{i\omega\sigma c}}{c\sinh(\sqrt{i\omega\sigma c})} \qquad g = \frac{\sqrt{i\omega\sigma c}}{c\tanh(\sqrt{i\omega\sigma c})}. \tag{11}$$

Note that when the storage of the leaky layer is neglected ($\sigma = 0$), both f and g equal $1/c$, and the equation for the flux through the leaky layer simplifies to $q_t = (h - h_0)/c$. Below the land, $h_0 = 0$, and the leakage $\tilde{q}_t$ simplifies to

$$\tilde{q}_t = \tilde{g}h, \tag{12}$$

where $\tilde{g}$ is obtained from (11) by replacing σ and c by $\tilde{\sigma}$ and $\tilde{c}$, respectively.

Substitution of (9) for h and (10) for q_t into (1), division of all terms by $e^{i\omega t}$, and combination of terms give the following differential equation for ϕ below the sea

$$T\frac{d^2\phi}{dx^2} = (g + i\omega S)\phi - [f + (g - f)\gamma + i\omega S\beta]h_s \quad x \le 0. \tag{13}$$

Similarly, the differential equation for ϕ below the land becomes

$$\tilde{T}\frac{\mathrm{d}^2\phi}{\mathrm{d}x^2} = (\tilde{g} + i\omega\tilde{S})\phi \quad x \geq 0. \tag{14}$$

A particular solution ϕ_p to the nonhomogeneous differential equation (13) is obtained from inspection as

$$\phi_p = \frac{f + (g - f)\gamma + i\omega S\beta}{g + i\omega S} h_s. \tag{15}$$

Note that when the aquifer is covered by an impermeable layer ($c = \infty$), both f and g are equal to zero, and $\phi_p = \beta h_s$. The general solution to the homogeneous form of (13) is

$$\phi = a\mathrm{e}^{x\sqrt{\alpha}} + b\mathrm{e}^{-x\sqrt{\alpha}}, \tag{16}$$

where a and b are constants and α is defined as

$$\alpha = \frac{g + i\omega S}{T}. \tag{17}$$

The general solution to the differential equation (14) has the same form as (16), but α is replaced by $\tilde{\alpha}$

$$\tilde{\alpha} = \frac{\tilde{g} + i\omega\tilde{S}}{\tilde{T}}. \tag{18}$$

Application of the boundary conditions (3) gives the following expressions for ϕ below the sea and the land

$$\begin{aligned} \phi &= \phi_p + a\mathrm{e}^{x\sqrt{\alpha}} \qquad x \leq 0 \\ \phi &= b\mathrm{e}^{-x\sqrt{\tilde{\alpha}}} \qquad x \geq 0. \end{aligned} \tag{19}$$

The constants a and b are obtained from condition (4), which give, using (9)

$$\begin{aligned} \phi_p + a &= b \\ -Ta\sqrt{\alpha} &= \tilde{T}b\sqrt{\tilde{\alpha}}. \end{aligned} \tag{20}$$

Solution of this system of two equations gives

$$a = \frac{-\tilde{T}\sqrt{\tilde{\alpha}}}{T\sqrt{\alpha} + \tilde{T}\sqrt{\tilde{\alpha}}}\phi_p \qquad b = \frac{T\sqrt{\alpha}}{T\sqrt{\alpha} + \tilde{T}\sqrt{\tilde{\alpha}}}\phi_p. \tag{21}$$

The final solution may now be written as

$$\begin{aligned} h &= \left(\phi_p + a\mathrm{e}^{x\sqrt{\alpha}}\right)\mathrm{e}^{i\omega t} \qquad x \leq 0 \\ h &= b\mathrm{e}^{-x\sqrt{\tilde{\alpha}}}\mathrm{e}^{i\omega t} \qquad x \geq 0. \end{aligned} \tag{22}$$

The real part of the above expression is the head fluctuation in the aquifer caused by a sea level that varies as a cosine function (7), while the imaginary part is the head fluctuation caused by a sea level that varies as a sine function (8). Note that the part of solution (22) for the aquifer below the land may be modified to obtain a solution for an aquifer that ends abruptly at the shore by replacing b by h_s.

The head in response to sinusoidal forcing may be defined by the amplitude and phase shift. For this purpose, the equation for the (complex) head (22) is written as

$$h = (u + iv)\mathrm{e}^{i\omega t} = \rho\mathrm{e}^{i\omega(t-\theta)}, \tag{23}$$

where u and v are the real and imaginary parts of $\phi(x)$ (19), ρ is the amplitude of the periodic variation at x, and θ is the phase shift at x

$$\rho = \sqrt{u^2 + v^2} \qquad \theta = -\frac{1}{\omega}\arctan(v/u). \tag{24}$$

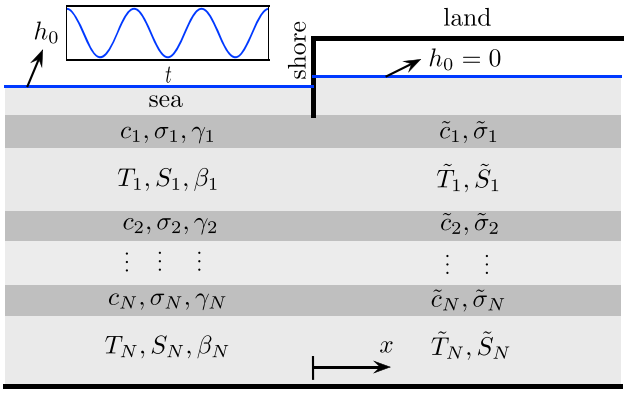

Figure 2. Cross section of a coastal aquifer consisting of N aquifer layers and N leaky layers.

3. Multilayer Solution

The solution for a single layer is extended to multiple layers using matrix calculus. Consider a coastal aquifer system consisting of a sequence of N aquifer layers and N leaky layers; leaky layer n is on top of aquifer layer n (Figure 2). The resistance to vertical flow is neglected within aquifer layers (Dupuit approximation), and flow in leaky layers is approximated as vertical. Below the sea, aquifer layer n has transmissivity T_n, storage coefficient S_n, and loading efficiency β_n, while leaky layer n has resistance to vertical flow c_n, storage coefficient σ_n, and loading efficiency γ_n. Below the land, all aquifer and leaky layer parameters have a tilde, and the loading efficiency is not of concern as the load on the aquifer does not vary.

Flow in aquifer layer n below the sea is governed by (cf. (1))

$$T_n \frac{\partial^2 h_n}{\partial x^2} = S_n \frac{\partial h_n}{\partial t} + q_{n,b} - q_{n+1,t} - S_n \beta_n \frac{\mathrm{d}h_0}{\mathrm{d}t} \qquad x \le 0, \tag{25}$$

where the upward leakage through the top of aquifer layer n is equal to the flux $q_{n,b}$ at the bottom of leaky layer n and the upward leakage through the bottom of aquifer layer n is equal to the flux $q_{n+1,t}$ at the top of leaky layer $n + 1$ (see Figure A1 in Appendix A). The latter equals zero for an impermeable bottom.

A solution for the head is again sought in complex form, similar to the derivation for one-dimensional flow. The net vertical outflow of each aquifer $(q_{n,b} - q_{n+1,t})$ may be expressed in complex form as a linear combination of the complex head in the aquifer and the complex heads in the aquifer layers above and below the aquifer, as derived in Appendix A. Substitution of (A16) for the complex net vertical outflow of each aquifer layer and combining all equations in one matrix differential equation for flow below the sea gives

$$\mathbf{T}\frac{\partial^2 \vec{h}}{\partial x^2} = \mathbf{S}\frac{\partial \vec{h}}{\partial t} + \mathbf{F}\vec{h} - \mathbf{G}\vec{h}_0 - \mathbf{SB}\frac{\mathrm{d}\vec{h}_0}{\mathrm{d}t} \qquad x \le 0, \tag{26}$$

where $\vec{h}$ is a column vector with the complex head in each aquifer layer, and $\vec{h}_0$ is a column vector with the complex fluctuation of the sea level.

$$\vec{h} = \begin{pmatrix} h_1 \\ h_2 \\ \vdots \\ h_N \end{pmatrix} \qquad \vec{h}_0 = \begin{pmatrix} h_s \\ h_s \\ \vdots \\ h_s \end{pmatrix} e^{i\omega t} = \vec{h}_s e^{i\omega t}. \tag{27}$$

T, **S**, and **B** are diagonal matrices with the values of the transmissivities T_n, storage coeffients S_n, and loading efficiencies β_n of the different layers on the diagonals. Matrix **F** is defined as

$$\mathbf{F} = \begin{pmatrix} g_1 + g_2 & -g_2 & 0 & \dots & 0 \\ -f_2 & g_2 + g_3 & -g_3 & \dots & 0 \\ \vdots & \ddots & \ddots & \ddots & \vdots \\ 0 & \dots & -f_{N-1} & g_{N-1} + g_N & -g_N \\ 0 & \dots & & -f_N & g_N \end{pmatrix}, \tag{28}$$

where f and g are given by (A13). Matrix $\mathbf{G}$ is a diagonal matrix with terms

$$G[n,n] = (g_n - f_n)\gamma_n + (g_{n+1} - f_{n+1})\gamma_{n+1} \qquad n = 2, \ldots, N-1, \tag{29}$$

except for the first and last rows

$$G[1,1] = f_1 + (g_1 - f_1)\gamma_1 + (g_2 - f_2)\gamma_2 \qquad G[N,N] = (g_N - f_N)\gamma_N. \tag{30}$$

The system of differential equations governing flow below the land is the same as (26), except that $\vec{h}_0 = 0$, and diagonal matrices $\mathbf{T}$, $\mathbf{S}$, and $\mathbf{F}$ are replaced by their equivalents with a tilde

$$\tilde{\mathbf{T}}\frac{\partial \vec{h}}{\partial x} = \tilde{\mathbf{S}}\frac{\partial \vec{h}}{\partial t} + \tilde{\mathbf{F}}\vec{h}. \tag{31}$$

Boundary conditions at infinity and conditions at the shore are the same as for the one-layer case ((3) and (4)) and may be written in vector form as

$$\begin{aligned} \frac{\partial \vec{h}}{\partial x} &= 0 \qquad x \to -\infty \\ \vec{h} &= 0 \qquad x \to \infty, \end{aligned} \tag{32}$$

and

$$\begin{aligned} \vec{h}(0^-, t) &= \vec{h}(0^+, t) \\ -\mathbf{T}\frac{\partial \vec{h}}{\partial x}(0^-, t) &= -\tilde{\mathbf{T}}\frac{\partial \vec{h}}{\partial x}(0^+, t). \end{aligned} \tag{33}$$

Solutions to matrix differential equations may be obtained using matrix differential calculus (e.g., Maas, 1986). A solution to the stated problem is sought again in separated form as

$$\vec{h} = \vec{\phi} e^{i\omega t}, \tag{34}$$

where $\vec{\phi}$ is a vector of functions that depend on x only. Substitution of this equation for $\vec{h}$ in the matrix differential equations (26) and (31), division of all terms by $e^{i\omega t}$, and gathering terms gives

$$\mathbf{T}\frac{d^2\vec{\phi}}{dx^2} = (\mathbf{F} + i\omega\mathbf{S})\vec{\phi} - (\mathbf{G} + i\omega\mathbf{SB})\vec{h}_s \qquad x \le 0, \tag{35}$$

$$\tilde{\mathbf{T}}\frac{d^2\vec{\phi}}{dx^2} = (\tilde{\mathbf{F}} + i\omega\tilde{\mathbf{S}})\vec{\phi} \qquad x \ge 0. \tag{36}$$

A particular solution to the nonhomogeneous matrix differential equation below the sea (35) is obtained from inspection as

$$\vec{\phi}_p = (\mathbf{F} + i\omega\mathbf{S})^{-1}(\mathbf{G} + i\omega\mathbf{SB})\vec{h}_s, \tag{37}$$

where $()^{-1}$ stands for the inverse of a matrix. The matrix $\mathbf{A}$ is introduced so that the homogeneous form of the matrix differential equation below the sea (35) becomes

$$\frac{d^2\vec{\phi}}{dx^2} = \mathbf{A}\vec{\phi}, \tag{38}$$

where

$$\mathbf{A} = \mathbf{T}^{-1}(\mathbf{F} + i\omega\mathbf{S}). \tag{39}$$

The general solution to this homogeneous matrix differential equation may be written as

$$\vec{\phi} = \exp(x\sqrt{\mathbf{A}})\vec{a} + \exp(-x\sqrt{\mathbf{A}})\vec{b}, \tag{40}$$

where the exponential and square root functions in this equation are matrix functions (see, e.g., Maas, 1986). Matrix exponential and square root functions are available in many libraries, including the SciPy package

for Python (Jones et al., 2018). The general solution to the differential equation for ϕ below the land (36) has the same form as (40), but the matrix $\mathbf{A}$ needs to be replaced by $\tilde{\mathbf{A}}$

$$\tilde{\mathbf{A}} = \tilde{\mathbf{T}}^{-1}(\tilde{\mathbf{F}} + i\omega\tilde{\mathbf{S}}). \tag{41}$$

Application of the boundary conditions (32) and addition of the particular solution below the sea (37) gives the following expressions for $\vec{\phi}$ below the sea and below the land

$$\begin{aligned} \vec{\phi} &= \vec{\phi}_p + \exp(x\sqrt{\mathbf{A}})\vec{a} \qquad x \le 0 \\ \vec{\phi} &= \exp(-x\sqrt{\tilde{\mathbf{A}}})\vec{b} \qquad x \ge 0. \end{aligned} \tag{42}$$

The vectors $\vec{a}$ and $\vec{b}$ are determined from the conditions at the shore line (33), which give, using (34)

$$\begin{aligned} \vec{\phi}_p + \vec{a} &= \vec{b} \\ -\mathbf{T}\sqrt{\mathbf{A}}\vec{a} &= \tilde{\mathbf{T}}\sqrt{\tilde{\mathbf{A}}}\vec{b}. \end{aligned} \tag{43}$$

Solution of this system of two equations gives

$$\vec{a} = -[(\tilde{\mathbf{T}}\sqrt{\tilde{\mathbf{A}}})^{-1}\mathbf{T}\sqrt{\mathbf{A}} + \mathbf{I}]^{-1}\vec{\phi}_p, \tag{44}$$

$$\vec{b} = [(\mathbf{T}\sqrt{\mathbf{A}})^{-1}\tilde{\mathbf{T}}\sqrt{\tilde{\mathbf{A}}} + \mathbf{I}]^{-1}\vec{\phi}_p, \tag{45}$$

where $\mathbf{I}$ is the identity matrix. The final solution is

$$\begin{aligned} h &= [\vec{\phi}_p + \exp(x\sqrt{\mathbf{A}})\vec{a}]e^{i\omega t} \qquad x \le 0 \\ h &= \exp(-x\sqrt{\tilde{\mathbf{A}}})\vec{b}e^{i\omega t} \qquad x \ge 0. \end{aligned} \tag{46}$$

As for the one-layer solution, the real part of the above expressions is the head fluctuation in the aquifer system caused by a sea level that varies as (7), while the imaginary part is the head fluctuation caused by a sea level that varies as (8). Note that the part of solution (46) for the aquifer system below the land may be modified to obtain a solution for an aquifer system that ends abruptly at the shore by replacing $\vec{b}$ by $\vec{h}_s$.

For the case that two aquifers are not separated by a leaky layer, the vertical flux between two aquifer layers may be computed with a simple finite difference scheme (e.g., Bakker, 2013b; Harbaugh, 2005). For example, the vertical flux q_z between aquifer layer n and aquifer layer $n-1$ is computed as

$$q_z = \frac{h_n - h_{n-1}}{c_n}, \tag{47}$$

where c_n is the resistance to vertical flow between the middle of aquifer layer n and the middle of aquifer layer $n-1$

$$c_n = \frac{H_n}{2k_{v,n}} + \frac{H_{n-1}}{2k_{v,n-1}}, \tag{48}$$

where H_n is the thickness of aquifer layer n, and $k_{v,n}$ is the vertical hydraulic conductivity of aquifer layer n. Two aquifer layers that are not separated by a leaky layer may be simulated with the presented solution (46) by specifying c_n with the equation given above and by setting the storage σ_n equal to zero.

4. Examples

The presented solutions for single-layer (22) and multilayer (46) aquifers are implemented in Python. Accurate numerical derivatives are used to verify that the presented solutions are indeed solutions to the stated differential equations and that the boundary conditions are met. The solution for a single layer has been evaluated extensively in a number of papers (e.g., Chuang & Yeh, 2007; Li et al., 2008). The examples presented here concern multilayer systems. Three examples are presented. First, the consistency of both the

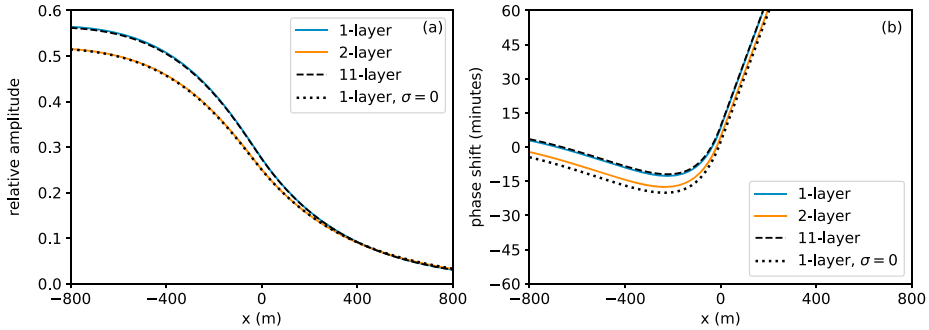

Figure 3. Comparison of models for tidal propagation in an aquifer covered by a thick clay layer for tide with a period of $\tau = 0.5$ d. (a) Amplitude and (b) Phase shift. Single-layer model (blue), 2-layer model (red), 11-layer model (black dash), and single-layer model with zero storage in leaky layer (black dotted).

mathematical derivation and numerical implementation of the presented single-layer and multilayer solutions is verified by using the multilayer solution to simulate flow in an aquifer covered by a thick clay layer. Second, the multilayer solution is used to investigate the tidal propagation in the deeper part of an unconfined aquifer, and the results are compared to the single-layer solution. In the third and final example, the effect of thin clay lenses on tidal propagation is studied.

4.1. Coastal Aquifer With a Thick Clay Layer

The objective of this example is to demonstrate the consistency between the single-layer and multilayer solutions. Consider a coastal aquifer covered by a thick clay layer. The thickness of both the clay layer and the aquifer is 20 m. The specific storage coefficient of both layers is $5 \cdot 10^{-5}$ m^{-1}. The hydraulic conductivity of the aquifer is 50 m/d, while the hydraulic conductivity of the clay layer is 5 mm/d (resistance is $c = 4,000$ d). The loading efficiency of the clay layer is 1 and of the aquifer 0.5. A tidal period of 0.5 d is considered, and the amplitude in the sea is h_s; computed amplitudes are presented relative to the amplitude in the sea. To test the consistency of the mathematical derivation and the Python implementation, the system is simulated as a multilayer solution where the clay layer is simulated as one or more aquifer layers. The multilayer solution is compared to the solution for a one-layer system covered by a leaky layer (which is computed with (22)).

The amplitude as a function of x is presented in Figure 3a and the phase shift as a function of x in Figure 3b. Four curves are shown. The blue curve is for the single-layer model. The red curve is for a two-layer model, where the leaky layer is modeled as one aquifer layer. This solution is inaccurate, as expected, because the vertical flux through the leaky layer and the storage in the leaky layer are modeled inaccurately when it is simulated with one aquifer layer. The two-layer solution is very similar to the single-layer solution when the storage in the leaky layer is set to zero, which is shown in the figure with the dotted line. The flow through the leaky layer can be modeled accurately with aquifer layers when the leaky layer is simulated with multiple aquifer layers. The black dashed line represents the solution when the leaky layer is modeled with 10 aquifer layers. This solution approaches the single-layer solution (the black dashed line overlays the blue line).

A few interesting characteristics of the accurate solution (blue and black dashed curves) are noted. The relative amplitude (Figure 3a) approaches 0.55 far away below the sea, while the loading efficiency of the aquifer is 0.5. This is caused by the resistance and storage of the leaky layer. When the storage of the leaky layer is set to zero, the amplitude far away below the sea approaches 0.5 up to three significant digits. When the resistance of the leaky layer is also increased, the amplitude is indeed 0.5 far away below the sea (not shown), as in the solution of Van der Kamp (1972). Far away below the land, the amplitude approaches zero (boundary condition). For the current case, after a few hundred meters, there is very little difference between the four models below the land.

The phase shift approaches 8.5 min far away below the sea (Figure 3b). Near the shore below the sea, the phase shift is actually negative, after which it starts increasing rapidly below the land. The phase shift above 60 min is not shown, but it keeps increasing linearly with distance from the shore. When the resistance of the leaky layer is increased and the storage of the leaky layer is set to zero, the phase shift far from the shore below the sea approaches zero, but the negative phase shift near the shore below the sea remains (not shown). Note that the amplitude and phase shift are a function of the tidal period. For the current example,

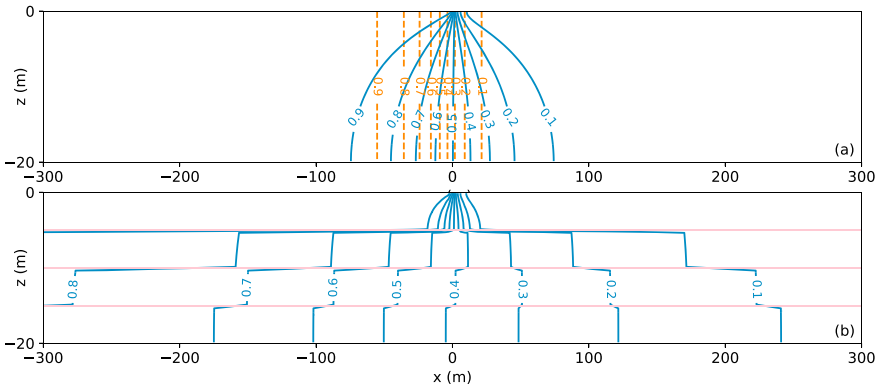

Figure 4. (a) Contours of the relative amplitude in a homogeneous unconfined aquifer for a tidal period of $\tau = 0.5$ d. Single-layer model (red dash) and 80-layer model (blue). (b) Contours of the relative amplitude when three thin clay layers of 25 cm (pink) are present in the aquifer.

a tide with a tidal period of $\tau = 0.5$ d damps out to 10% at a distance of approximately 370 m (Figure 3), while a tide with a tidal period of $\tau = 28$ d damps out to 10% at approximately 2,450 m.

The comparisons of Figure 3 demonstrate that the derivation and implementation of the single-layer and multilayer solutions are consistent: They give the same answer when the leaky layer is simulated with enough leaky layers, which also gives a solution for the head in the leaky layer. In practice, it is, of course, more efficient to simply model it as one leaky layer, unless the head in the leaky layer is of interest.

4.2. Tidal Propagation in an Unconfined Aquifer

The objective of the second example is to investigate how the tidal signal propagates in the deeper part of an unconfined aquifer. Consider an unconfined aquifer with (approximately constant) aquifer thickness $H = 20$ m, a horizontal hydraulic conductivity of 10 m/d, a vertical hydraulic conductivity of $k_v = 1$ m/d, a phreatic storage of 0.1, an elastic storage of $5 \cdot 10^{-5}$ m^{-1}, and a loading efficiency of 0.8. There is no leaky seabed.

First, the aquifer is modeled as a single layer. The vertical flux between the aquifer and the sea is computed with (47) as $q_z = (h - h_0)/c$ where $c = 0.195H/k_v$; this effective value of c results in the correct discharge in steady models (Anderson, 2005). The storage coefficient for the aquifer below the land is specified as 0.1. The amplitude of a tide with period $\tau = 0.5$ d is computed as a function of x with (22). The relative amplitude is contoured and shown with the red dashed lines in Figure 4a.

Next, the same aquifer is simulated with a multilayer model consisting of 80 layers of equal thickness of 25 cm. The top layer of the aquifer below the land has a storage coefficient of 0.1, while the other 79 layers have a storage coefficient of $1.25 \cdot 10^{-5}$. (This approach of simulating a phreatic aquifer was applied by

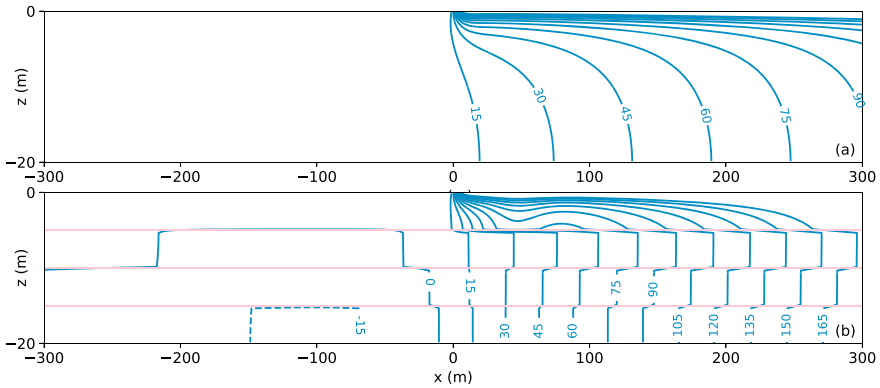

Figure 5. Contours of the phase shift (minutes) in an unconfined aquifer modeled with 80 layers and a tidal period of $\tau = 0.5$ d. (a) Homogeneous aquifer and (b) aquifer with three thin clay lenses of 25 cm (shown in pink).

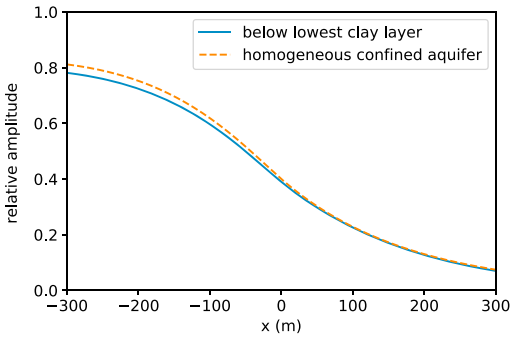

Figure 6. The amplitude at the bottom of the unconfined aquifer with three clay lenses of Figure 4b (blue) versus the amplitude in a homogeneous confined aquifer of the same total transmissivity and storage (red dash).

Bakker, 2013a, to simulate the solution for transient flow to a partially penetrating well in an unconfined aquifer of Neuman, 1972.) Contours of the relative amplitude are shown with the blue contours in Figure 4a, and contours of the phase shift (in minutes) are shown in Figure 5a. This example demonstrates that the amplitude and phase shift vary significantly in the vertical direction in an unconfined aquifer.

4.3. Tidal Propagation in an Unconfined Aquifer With Clay Lenses

Consider the unconfined aquifer of the previous example, but now there are three 25-cm-thick clay lenses. The clay lenses are simulated as leaky layers. The vertical hydraulic conductivity of the clay lenses is 1 mm/d so that the resistance of the clay lenses is 250 days. The storage coefficient of the clay lenses is $1.25 \cdot 10^{-5}$ (the same as the aquifer layers), and the loading efficiency of the clay lenses is 1. Contours of the relative amplitude are shown in Figure 4b. Note the effect of the three thin clay lenses. The 0.1 relative amplitude contour propagates approximately three times as far at the bottom of the aquifer as compared to the unconfined aquifer without the clay lenses. In fact, the propagation in the bottom part of the aquifer approaches the propagation in a confined aquifer of the same total thickness and total storage of the aquifer, especially in the aquifer below the land (Figure 6).

The phase shift for the case with clay layers is contoured in Figure 5b. The clay layers have a large effect on the contours of the phase shift. Below the land, the phase shift decreases with depth until below the first clay lens, after which it increases again below the deeper clay lenses. In the part of the aquifer above the first clay layer, the phase shift shows a curious variation, as it increases with distance from the shore, then decreases and then increases again. This behavior is caused by the interaction with the deeper layers through the clay layer, but it is not important for this example, as this happens at a distance from the shore where the remaining amplitude is negligibly small (see Figure 4b).

5. Conclusions and Discussion

A new multilayer solution was presented for tidal propagation in a coastal aquifer. Many of the existing solutions, as cited in section 1, are special cases of the solution presented here. The solution was obtained using matrix calculus and can be applied to an arbitrary number of layers. The amplitude and phase shift can be computed analytically in every layer. It was shown that the tidal propagation can vary significantly in the vertical direction in both homogeneous unconfined aquifers and even more pronounced in unconfined aquifers with thin clay lenses. Below the clay lenses of the presented example, the amplitude approaches that of a confined aquifer.

Application to field measurements is beyond the scope of this paper, but it was demonstrated that the depth at which the propagation of the tidal signal is measured is critical. Similarly, thin layers of low permeability have a large impact on observations. As a result, the accurate estimation of aquifer parameters from tidal propagation in coastal aquifers is challenging. It will require deep knowledge of the system heterogeneity (e.g., from drilling the observation wells) and will likely result in the estimation of lumped parameters.

For unconfined flow, the transmissivity in the aquifer below the land was approximated as constant. This is a reasonable approximation when the tidal fluctuation is small relative to the saturated thickness of the unconfined aquifer (e.g., Sheets et al., 2015). The loading effect caused by variations in the top part of an unconfined aquifer were neglected in the aquifer below the land, although the presented solution can be modified to include this effect. Wang et al. (2012) studied these effects and concluded that the loading effect of water table variations enhances the amplitude and reduces the phase shift when the water table aquifer is separated from the underlying aquifer by an impermeable layer. Effects of density variations because of salinity variations were also neglected. This effect was also studied by Wang et al. (2012), who concluded that for their setup, the error in the amplitude caused by neglecting density differences was less than 2.5%. Finally, the analysis presented in this paper was based on the standard approximation in groundwater mechanics that there are no horizontal deformations in the aquifer, leading to differential equation (1). Other approximations are possible that allow for horizontal deformations (e.g., Boutt, 2010; Verruijt, 2015), which deserve further attention.

Appendix A: Flow Through Leaky Layer

The objective of this appendix is to derive equations for the vertical flux at the top and bottom of a leaky layer in terms of the heads in the aquifer layers below and above the leaky layer while taking into account storage in the leaky layer. Hemker and Maas (1987) and Bakker (2013a) performed a similar analysis in the Laplace domain. Consider leaky layer n between aquifer layers $n-1$ (top) and n (bottom) below the sea (Figure A1).

Leaky layer n has vertical hydraulic conductivity κ_n, specific storage coefficient $\sigma_{s,n}$, thickness D_n, and loading efficiency γ_n. Flow in the leaky layer is approximated as vertical. The head in the leaky layer is governed by

$$\kappa_n \frac{\partial^2 h}{\partial z^2} = \sigma_{s,n} \frac{\partial h}{\partial t} - \sigma_{s,n} \gamma_n \frac{\mathrm{d}h_0}{\mathrm{d}t}, \tag{A1}$$

where h_0 is the fluctuation of the sea level. Local vertical coordinate z varies from 0 at the bottom of leaky layer n to D_n at the top of leaky layer n. Differential equation A1 may be written as

$$\frac{\partial^2 h}{\partial z^2} = \frac{\sigma_n c_n}{D_n^2} \left(\frac{\partial h}{\partial t} - \gamma_n \frac{\mathrm{d}h_0}{\mathrm{d}t} \right), \tag{A2}$$

where $c_n = D_n/\kappa_n$ is the resistance to vertical flow of the leaky layer, and $\sigma_n = \sigma_{s,n} D_n$ is the storage coefficient of the leaky layer.

The fluctuation of the sea level is written in complex form (5). Boundary conditions are that the complex heads at the bottom and top of the leaky layer are equal to the complex heads in the aquifer layers below and above, respectively, written in the form (9)

$$h(z=0) = \phi_n \mathrm{e}^{i\omega t} \qquad h(z=D_n) = \phi_{n-1} \mathrm{e}^{i\omega t}. \tag{A3}$$

A solution is sought in the form

$$h = \phi \mathrm{e}^{i\omega t}, \tag{A4}$$

where ϕ is a (complex) function of z only. Substitution of (A4) for h in (A2), division of all terms by $\mathrm{e}^{i\omega t}$, and combination of terms give

$$\frac{\mathrm{d}^2 \phi}{\mathrm{d}z^2} = \frac{i\omega \sigma_n c_n}{D_n^2} \left(\phi - \gamma_n h_\mathrm{s} \right), \tag{A5}$$

with boundary conditions

$$\phi(z=0) = \phi_n \qquad \phi(z=D_n) = \phi_{n-1}. \tag{A6}$$

The solution for ϕ is straightforward (e.g., Bakker, 2013a; Strack, 1989)

$$\phi = \frac{(\phi_{n-1} - \gamma_n h_\mathrm{s}) \sinh(\lambda_n z/D_n) + (\phi_n - \gamma_n h_\mathrm{s}) \sinh[\lambda_n (1 - z/D_n)]}{\sinh(\lambda_n)} + \gamma_n h_\mathrm{s}, \tag{A7}$$

where

$$\lambda_n = \sqrt{i\omega \sigma_n c_n}, \tag{A8}$$

and the vertical gradient is

$$\frac{\mathrm{d}\phi}{\mathrm{d}z} = \frac{\frac{\lambda_n}{D_n}(\phi_{n-1} - \gamma_n h_\mathrm{s}) \cosh(\lambda_n z/D_n) - \frac{\lambda_n}{D_n}(\phi_n - \gamma_n h_\mathrm{s}) \cosh[\lambda_n (1 - z/D_n)]}{\sinh(\lambda_n)}. \tag{A9}$$

The vertical components of the specific discharge at the bottom ($q_{n,b}$) and top ($q_{n,t}$) of leaky layer n may now be obtained with Darcy's law and through multiplication with $\mathrm{e}^{i\omega t}$

$$q_{n,b} = -\kappa_n \frac{\mathrm{d}\phi}{\mathrm{d}z}(z=0) \mathrm{e}^{i\omega t} \qquad q_{n,t} = -\kappa_n \frac{\mathrm{d}\phi}{\mathrm{d}z}(z=D_n) \mathrm{e}^{i\omega t}. \tag{A10}$$

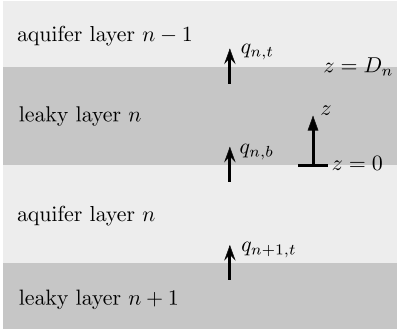

Figure A1. Flux into and out of leaky layer n and aquifer layer n.

Combination of (A9) and (A10) gives, after some rearrangement of terms

$$q_{n,b} = g_n h_n - f_n h_{n-1} - (g_n - f_n)\gamma_n h_0, \tag{A11}$$

$$q_{n,t} = f_n h_n - g_n h_{n-1} - (f_n - g_n)\gamma_n h_0, \tag{A12}$$

where

$$f_n = \frac{\lambda_n}{c_n \sinh(\lambda_n)} \qquad g_n = \frac{\lambda_n}{c_n \tanh(\lambda_n)}. \tag{A13}$$

Note that for the case that the storage in the leaky layer is zero, $\lambda_n = 0$, and f_n and g_n are

$$\lim_{\lambda \to 0} f_n = \lim_{\lambda \to 0} g_n = 1/c_n, \tag{A14}$$

so that the flux at the bottom and top of the leaky layer can be computed as the head difference between the aquifer layers divided by the resistance of the leaky layer.

For a single aquifer, the complex flux out of the top of the aquifer is equal to the flux at the bottom of leaky layer 1 and may be written as

$$q_{1,b} = g_1 h_1 - [f_1 + (g_1 - f_1)\gamma_1]h_0. \tag{A15}$$

The flux out of the top of aquifer layer n is equal to the flux at the bottom of leaky layer n, while the flux out of the bottom of aquifer layer n is equal to minus the flux at the top of leaky layer $n + 1$ (Figure A1), so that the complex net vertical outflow from aquifer layer n may be written as

$$\begin{aligned} q_{n,b} - q_{n+1,t} = &- f_n h_{n-1} + (g_n + g_{n+1})h_n - f_{n+1}h_{n+1} - \\ &[(g_n - f_n)\gamma_n + (g_{n+1} - f_{n+1})\gamma_{n+1}]h_0. \end{aligned} \tag{A16}$$

Acknowledgments
This research is part of NWO project Delta MAR, W 07.69.107. The presented solution is implemented in Python, and all examples are written as Jupyter Notebooks. The code and notebooks are available at github.com/mbakker7/maqtides under the MIT license.

References

Anderson, E. I. (2005). Modeling groundwater-surface water interactions using the Dupuit approximation. *Advances in Water Resources*, *28*, 315–327.

Bakker, M. (2004). Transient analytic elements for periodic Dupuit-Forchheimer flow. *Advances in Water Resources*, *27*(1), 3–12.

Bakker, M. (2013a). Analytic modeling of transient multi-layer flow. In P. Mishra, & K. Kuhlman (Eds.), *Advances in hydrogeology* (pp. 95–114). Heidelberg: Springer.

Bakker, M. (2013b). Semi-analytic modeling of transient multi-layer flow with TTim. *Hydrogeology Journal*, *21*, 935–943.

Bakker, M. (2016). The effect of loading efficiency on the groundwater response to water level changes in shallow lakes and streams. *Water Resources Research*, *52*, 1705–1715. https://doi.org/10.1002/2015WR017977

Boutt, D. F. (2010). Poroelastic loading of an aquifer due to upstream dam releases. *Groundwater*, *48*(4), 580–592.

Carr, P. A., & Van Der Kamp, G. S. (1969). Determining aquifer characteristics by the tidal method. *Water Resources Research*, *5*(5), 1023–1031.

Chuang, M. H., & Yeh, H. D. (2007). An analytical solution for the head distribution in a tidal leaky confined aquifer extending an infinite distance under the sea. *Advances in water resources*, *30*(3), 439–445.

Chuang, M. H., & Yeh, H. D. (2008). Analytical solution for tidal propagation in a leaky aquifer extending finite distance under the sea. *Journal of Hydraulic Engineering*, *134*(4), 447–454.

Ferris, J. G. (1952). Cyclic fluctuations of water level as a basis for determining aquifer transmissibility. Ground-water hydraulics section, Contribution No. 1. US Geological Survey.

Harbaugh, A. W. (2005). MODFLOW-2005, the US Geological Survey modular ground-water model the ground-water flow process. U.S. Geol. Surv. Tech. Methods, 6-A16, variously paginated.

Hemker, C. J., & Maas, C. (1987). Unsteady flow to wells in layered and fissured aquifer systems. *Journal of Hydrology*, *90*, 231–249.

Hvorslev, M. J. (1951). Time lag and soil permeability in ground-water observations. US Army Corps of Engineers, Waterways Experiment Station, Vicksburg, Mississippi, Bulletin 36.

Jones, E., Oliphant, E., Peterson, P., & the SciPy community (2018). SciPy: Open source scientific tools for Python. http://www.scipy.org/, accessed 2018-11-28.

Li, G., & Chen, C. (1991). Determining the length of confined aquifer roof extending under the sea by the tidal method. *Journal of Hydrology*, *123*, 97–104.

Li, H., & Jiao, J. J. (2001). Tide-induced groundwater fluctuation in a coastal leaky confined aquifer system extending under the sea. *Water Resources Research*, *37*(5), 1165–1171.

Li, H., & Jiao, J. J. (2003). Review of analytical studies of tidal groundwater flow in coastal aquifer systems, *Proceedings of the International Symposium on Water Resources and the Urban Environment* (pp. 86–91). PR China: Wuhan.

Li, G., Li, H., & Boufadel, M. C. (2008). The enhancing effect of the elastic storage of the seabed aquitard on the tide-induced groundwater head fluctuation in confined submarine aquifer systems. *Journal of hydrology*, *350*(1-2), 83–92.
Li, H., Li, G., Cheng, J., & Boufadel, M. C. (2007). Tide-induced head fluctuations in a confined aquifer with sediment covering its outlet at the sea floor. *Water Resources Research*, *43*, W03404. https://doi.org/10.1029/2005WR004724
Maas, C. (1986). The use of matrix differential calculus in problems of multiple-aquifer flow. *Journal of Hydrology*, *88*(1-2), 43–67.
Maas, C., & De Lange, W. J. (1987). On the negative phase shift of groundwater tides near shallow tidal rivers: The Gouderak anomaly. *Journal of Hydrology*, *92*(3-4), 333–349.
Neuman, S. P. (1972). Theory of flow in unconfined aquifers considering delayed response of the water table. *Water Resources Research*, *8*(4), 1031–1045.
Nielsen, P. (1990). Tidal dynamics of the water table in beaches. *Water Resources Research*, *26*(9), 2127–2134.
Pool, M., Post, V. E., & Simmons, C. T. (2014). Effects of tidal fluctuations on mixing and spreading in coastal aquifers: Homogeneous case. *Water Resources Research*, *50*, 6910–6926. https://doi.org/10.1002/2014WR015534
Post, V. E. A. (2011). A new package for simulating periodic boundary conditions in MODFLOW and SEAWAT. *Computers & Geosciences*, *37*(11), 1843–1849.
Rotzoll, K., El Kadi, A. I., & Gingerich, S. B. (2008). Analysis of an unconfined aquifer subject to asynchronous dual-tide propagation. *Groundwater*, *46*(2), 239–250.
Sheets, R. A., Hill, M. C., Haitjema, H. M., Provost, A. M., & Masterson, J. P. (2015). Simulation of water-table aquifers using specified saturated thickness. *Groundwater*, *53*(1), 151–157.
Slooten, L. J., Carrera, J., Castro, E., & Fernandez-Garcia, D. (2010). A sensitivity analysis of tide-induced head fluctuations in coastal aquifers. *Journal of Hydrology*, *393*(3–4), 370–380.
Strack, O. D. L. (1989). *Groundwater mechanics*. Englewood Cliffs, NJ: Prentice Hall.
Su, N., Liu, F., & Anh, V. (2003). Tides as phase-modulated waves inducing periodic groundwater flow in coastal aquifers overlaying a sloping impervious base. *Environmental Modelling & Software*, *18*(10), 937–942.
Sun, P., Li, H., Boufadel, M. C., Geng, X., & Chen, S. (2008). An analytical solution and case study of groundwater head response to dual tide in an island leaky confined aquifer. *Water Resources Research*, *44*, W12501. https://doi.org/10.1029/2008WR006893
Teo, H. T., Jeng, D. S., Seymour, B. R., Barry, D. A., & Li, L. (2003). A new analytical solution for water table fluctuations in coastal aquifers with sloping beaches. *Advances in Water Resources*, *26*(12), 1239–1247.
Van der Kamp, G. (1972). Tidal fluctuations in a confined aquifer extending under the sea. *International Geology Cong.*, *24*, 101–106.
Vandenbohede, A., & Lebbe, L. (2007). Effects of tides on a sloping shore: Groundwater dynamics and propagation of the tidal wave. *Hydrogeology Journal*, *15*(4), 645–658.
Verruijt, A. (2015). Theory and problems of poroelasticity 266 pp. http://geo.verruijt.net
Wang, X., Li, H., Wan, L., Liu, F., & Jiang, X. (2012). Loading effect of water table variation and density effect on tidal head fluctuations in a coastal aquifer system. *Water Resources Research*, *48*, W09501. https://doi.org/10.1029/2011WR011600
Yeh, H. D., Huang, C. S., Chang, Y. C., & Jeng, D. S. (2010). An analytical solution for tidal fluctuations in unconfined aquifers with a vertical beach. *Water Resources Research*, *46*, W10535. https://doi.org/10.1029/2009WR008746